

Original Research Paper

pH Mediated Control Synthesis of Lanthanide-Doped YPO₄ Upconversion Nano/Microcrystals

¹Meiling Tan, ¹Shuwei Hao, ¹Xiangbin Meng, ¹Jing Liu, ¹Yunfei Shang,
^{1,2}Chunhui Yang and ^{1,3}Guanying Chen

¹School of Chemical Engineering and Technology, Harbin Institute of Technology, Harbin 150001, China

²Harbin Huigong Technology Co., Ltd., Harbin150001, China

³Institute for Lasers, Photonics and Biophotonics, The State University of New York at Buffalo, Buffalo, NY 14260, USA

Article history

Received: 30-03-2015

Revised: 25-04-2015

Accepted: 25-04-2015

Corresponding Authors:

Shuwei Hao and Guanying Chen
School of Chemical Engineering
and Technology, Harbin Institute
of Technology, Harbin 150001,
China

Institute for Lasers, Photonics and
Biophotonics, The State
University of New York at
Buffalo, Buffalo, NY 14260, USA
Email: chenguanying@hit.edu.cn/
haosw@hit.edu.cn

Abstract: A pH-mediated rational control over the phase transformation, morphology and size of lanthanide doped YPO₄ nano/microcrystals has been accomplished using a hydrothermal route. The morphology of the resulting particles evolves from the spheres, to the nanoflakes and finally to the nanorods when increasing the pH value of the reaction solution from 1 to 9, while the induction of crystal phase transformation from a tetragonal structure to a hexagonal structure takes place at pH = 5. When excited at 980 nm, the hexagonal phase YPO₄•0.8H₂O: 18%Yb³⁺, 2%Er³⁺ nanoflakes prepared at pH = 7 exhibit the strongest UC emission intensity among investigated samples of varying size, phase and morphologies. This work provides a paradigm on the controlled synthesis of lanthanide doped upconverting orthophosphates, which hold great promise for various photonic and biophotonic applications.

Keywords: Orthophosphate, Morphology, Upconversion

Introduction

Frequency Upconversion (UC) in nano/microcrystals doped with trivalent Lanthanide (Ln³⁺) ions has attracted wide attentions in recent years due to its potential application in many fields such as volumetric multicolor displays (Downing *et al.*, 1996), solar cells (Chen *et al.*, 2013a), bioimaging (Chen *et al.*, 2014; 2012), drug delivery (Hou *et al.*, 2011; Tian *et al.*, 2012) and photodynamic therapy (Shan *et al.*, 2011; Zhang *et al.*, 2007). They are able to convert two or more photons, typically Near Infrared (NIR) light, into shorter wavelength visible or ultraviolet emission (Chen *et al.*, 2014). To realize highly efficient UC emissions, various host matrices have been extensively studied to provide an appropriate local crystal field effect for the incorporated lanthanide ions, alongside their conspicuous physicochemical properties (Chen *et al.*, 2014). Among investigated Ln³⁺ doped nano/microcrystals of varying host lattices, the Ln³⁺ doped orthophosphates hold great promise in most of aforementioned technological applications, as the orthophosphate host lattice possesses excellent physicochemical and optical stabilities under high temperature and high energy excitations and

enables the Ln³⁺ ions to illuminate at a high efficiency (Balakrishnaiah *et al.*, 2009; Di *et al.*, 2007; 2005; Meyssamy *et al.*, 1999; 2001).

Previously, Ln³⁺ doped orthophosphate particles have been typically used as typical downconversion (or Stokes type) luminophores whereby the emission wavelength is longer than the excitation wavelength. They have been considered as one of the promising candidates for Plasma Display Panel (PDP) applications due to their high absorption, high thermal and chemical stabilities (Balakrishnaiah *et al.*, 2009; Di *et al.*, 2007; 2005). Hasse and co-workers have successfully synthesized LaPO₄ downconversion particles via wet-chemical method for such purpose, whereby the phase structure of resulting products was controlled by changing the temperature used for crystallization (Meyssamy *et al.*, 1999). A later work reported by the same group indicates that a luminescence quantum yield up to 61% can be achieved in this luminescent Ce³⁺/Tb³⁺ codoped downconversion nanoparticles (Meyssamy *et al.*, 2001)]. The reported low toxicity and luminescence stability allow these Ln³⁺ doped LaPO₄ to be potentially used as biolabels towards clinical practices (Hutchison 1999; de Sousa Filho and Serra, 2011; Meiser *et al.*, 2004).

The Ln^{3+} doped YPO_4 particles is an analogy of the Ln^{3+} doped LaPO_4 particles due to the similarities between the Y and the La rare earth element as well as the identical structures of both materials. Indeed, Li *et al.* (2009) reported that YPO_4 particles doped with Ln^{3+} ($\text{Ln} = \text{Tb}, \text{Eu}, \text{Dy}$) and V^{5+} ions nano/microcrystals have superior downconversion emissions. These results make both LaPO_4 and YPO_4 host materials attractive toward various optically related applications. However, all these reported works are related to the downconversion (or Stokes-shifted) emission properties (Luwang *et al.*, 2011; Mai *et al.*, 2007; Yang *et al.*, 2009; Li *et al.*, 2009). Limited attentions have been paid to the upconversion (or anti-Stokes shifted) luminescence of Ln^{3+} doped orthophosphate particles.

A pertinent attempt has been made to dope the sensitizer Yb^{3+} and the activator Er^{3+} into the bulk single crystal LaPO_4 host material. An efficient visible upconversion has been realized upon excitation at 980 nm in the codoped single crystal due to the efficient energy transfer from Yb^{3+} to Er^{3+} ions and the strong absorption ability of Yb^{3+} ions (Lisiecki *et al.*, 2009). In addition, intense NIR to visible frequency upconversion luminescence has also been reported in single Er^{3+} -doped YPO_4 phosphors (Balakrishnaiah *et al.*, 2010). Both results suggest that the LnPO_4 material is promising host lattice for Ln^{3+} ions to produce superior upconversion luminescence along the well-established fact on producing efficient downconversion luminescence. It is well known that the morphology, the phase structure and the size of the resulting particles are of particular importance for their performance to meet the needs for specific applications. These parameters also play a significant role in defining the upconverting luminescence properties, as manifested in Ln^{3+} doped fluoride particles (NaYF_4 , NaLuF_4 , LuF_3 , etc) (Dou and Zhang, 2011; Hao *et al.*, 2014; Li *et al.*, 2008; Hao *et al.*, 2012). However, till this moment, there lacks facile routes to synthesize and to rationally control the phase transformation, the morphology, as well as the size of Ln^{3+} doped YPO_4 upconverting nano/microparticles. Moreover, the impact of the morphology and phase on the UC luminescence from Ln^{3+} doped YPO_4 nano/microcrystals remained unexplored.

Herein, we report on the controlled synthesis of the tetragonal $\text{YPO}_4:18\%\text{Yb}^{3+},2\%\text{Er}^{3+}$ and the hexagonal $\text{YPO}_4 \cdot 0.8\text{H}_2\text{O}:18\%\text{Yb}^{3+},2\%\text{Er}^{3+}$ nano/microcrystals with uniform and tunable size via a hydrothermal route. It is worth noting that the common hydrophilic chelating agent of trisodium citrate (for the preparation of down conversion orthophosphate particles) is replaced by the lipophilic chelating agent of Oleic Acid (OA) in the current preparing procedure, which has seldom been

investigated before for the synthesis of Ln^{3+} doped YPO_4 particles. We demonstrate that the pH value of the reaction solution plays a significant role in determination of the morphology and the phase of the resulting $\text{YPO}_4: \text{Yb}^{3+}/\text{Er}^{3+}$ particles. Furthermore, we show that the hexagonal phase $\text{YPO}_4 \cdot 0.8\text{H}_2\text{O}:18\%\text{Yb}^{3+},2\%\text{Er}^{3+}$ nanoflakes exhibit the strongest UC emission intensity among the resulting particles of varying morphologies. Based on the observed 4f-4f transitions of trivalent lanthanide ions, we also discuss the possible upconverting pathways of the $\text{Yb}^{3+}/\text{Er}^{3+}$ codoped YPO_4 nano/micronanoparticles.

Experimental

All the reagents were purchased from Tianjin Chemical Reagents Co.Ltd. and used as raw materials without further purification.

About 1.2 g NaOH was firstly dissolved in 3 mL distilled H_2O under vigorous stir; after that 5 mL ethanol and 18 mL OA were added in order into the above aqueous solution. The agitation lasted 30 min before 2 mL of $\text{Ln}(\text{NO}_3)_3 \cdot 6\text{H}_2\text{O}$ (0.5 M) ($\text{Y}^{3+}:\text{Yb}^{3+}:\text{Er}^{3+} = 80:18:2$) was added into the above faint yellow viscous solution. After that, 2 mL of $\text{NH}_4\text{H}_2\text{PO}_4$ (1.5 M) was added into the above milky mixture in 10 min. Then the mixing solution was transferred into a 50 mL Teflon bottle held in a stainless steel autoclave, sealed tightly and maintained steadily at 180°C for 24 h. After cooling down to room temperature naturally, the precipitates were collected by centrifugation and washed with deionized water and ethanol in sequence for several time and then dried in air at 60°C for 12 h. The samples with various morphologies were synthesized using the same protocol and parameters except by adjusting the pH value of the reaction solution before transferring to the hydrothermal reactor (i.e., pH = 1, 3, 5, 7 and 9) via the adding NaOH (5 M) or HNO_3 (5 M). The synthesis process of hexagonal $\text{YPO}_4 \cdot 0.8\text{H}_2\text{O}$ submicroprisms referred to the literature procedure (Li *et al.*, 2009) with the difference in doping different types and amount of trivalent lanthanide ions.

The X-Ray powder Diffraction (XRD) pattern was carried out with a Rigaku D/max- γB diffractometer equipped with a rotating anode and a Cu K α source ($\lambda = 0.154056$ nm). Micrographs for the prepared samples were obtained using a Field Emission Scanning Electron Microscope (FESEM, MX2600FE). The as-prepared powders were pressed to form a smooth and flat disk to be utilized for spectral studies by irradiation with 980 nm diode laser (Hi-Tech Optoelectronics Co. Ltd, Beijing). The emitted UC fluorescence was collected by a lens-coupled monochromator (Zolix Instruments Co. Ltd, Beijing) of 2 nm spectral resolution with an attached photomultiplier tube (Hamamatsu CR131).

Results and Discussion

The pH value of the initial reaction solution exerts a large impact on the phase and morphology of the resulting Yb³⁺, Er³⁺ doped YPO₄ nano/microcrystals. The crystal phases of the resulting products were measured and identified by the XRD technique. The XRD patterns of the samples synthesized with the stabilizing agent of OA under different pH conditions (i.e., pH = 1, 3, 5, 7 and 9) are all shown in Fig. 1. As one can see in Fig. 1, a tetragonal YPO₄ structure is adopted for the products when the pH value is below 3 under the current synthesizing condition. However, when the pH value is increased from 3 to 5, a new hexagonal phase of YPO₄•0.8H₂O appears, manifesting the occurrence of a phase transformation. With further increasing the pH value to and exceeding 7, the pure hexagonal phase YPO₄•0.8H₂O (JCPDS No. 42-0082) particles were obtained. Therefore, it can be concluded that the change of pH value of the initial reaction solution can induce the phase transformation from the tetragonal phase to the hexagonal phase, along with dramatic morphology changes of the products (consulted Fig. 2). Moreover, Fig. 1 displays a large difference in the relative intensities of the XRD diffraction peaks for samples of either the tetragonal phase or the hexagonal phase, revealing a preferential orientation growth along some crystal directions. In particular, the resulting products prepared at pH equal or below 7 exhibit much stronger diffraction peak intensities than the sample prepared at pH = 9.

The FESEM images provide direct information about the shape and size of the Yb³⁺/Er³⁺ codoped YPO₄ samples prepared at different pH values (Fig. 2). The tetragonal phase YPO₄:18%Yb³⁺,2%Er³⁺ forms prepared at pH = 1, are round shape particles of 1 μm, defined by the aggregation of numerous nanoparticles (Fig. 2a). The type and concentration of lanthanide dopants were confirmed by energy dispersive x-ray spectrum (data not shown). When the pH is increased to 3, the tetragonal phase YPO₄:18%Yb³⁺,2%Er³⁺ forms tend to grow into regular shape nanoparticles with an average size of 90 nm, as shown in Fig. 2b. However, when the pH is equal to 5, significant change takes place in the morphology. Two distinct morphologies appear, including the small round shape nanoparticles (~90 nm) and the rod shape nanoparticles (90 nm × 1 μm), as shown in Fig. 2c. This observation is in good agreement with the XRD result of coexisting the tetragonal YPO₄:18%Yb³⁺,2%Er³⁺ phase and the hexagonal YPO₄•0.8H₂O:18%Yb³⁺,2%Er³⁺ phase at pH = 5 (Fig. 2). When the pH value of the reaction system is increased to 7, uniform nanoflakes were generated, as shown in Fig. 2d. The FESEM images of the sample synthesized at pH = 9 reveals the products are

nanorods shape (Fig. 2e). Compiling the results from the XRD and FESEM measurements, we can conclude that the pH value of the initial reaction solution play a vital role in determination of the phase and the morphology transition of the resulting particles. The higher pH value facilitates the formation of larger size particles with regular shape and lower crystal symmetry. The pH-induced morphology change can be attributed to the fact that the absorption abilities of the OA on certain crystal facets are regulated by the electrostatic interaction between the carboxylic group and the trivalent Ln³⁺ ions, which are very sensitive to the pH value of the reaction solution (Li *et al.*, 2007). It is known that the UC luminescence intensity is dependent on the phase, the size and morphology of the particles (Chen *et al.*, 2014). As a result, the pH-induced phase, size and morphology change will produce a pronounced effect on the UC luminescence intensity. Moreover, regular submicron sized hexagonal YPO₄•0.8H₂O prisms (Fig. 2f) were also synthesized using the commonly used hydrophilic trisodium citrate as a chelating agent, in order to provide a reference for optical comparison with the particles prepared in this work using the lipophilic OA as the chelating agent.

To evaluate the effect of the phase and morphology on the UC luminescent properties of YPO₄:18%Yb³⁺,2%Er³⁺ and YPO₄•0.8H₂O:18%Yb³⁺,2%Er³⁺ particles, the resulting samples were excited by a 980 nm laser with excitation power density of ~390 W/cm² at room temperature and all the signal were collected under exactly identical conditions (Fig. 3). The luminescence emission spectra of the resulting samples of varying morphology are discerned using color-encoded lines, the tetragonal phase nanoparticles prepared at pH = 3 (black line), the mixed tetragonal and hexagonal phase particles prepared at pH = 5 (red line), the hexagonal phase nanoflakes prepared at pH = 7 (blue line), the hexagonal phase nanorods prepared at pH = 9 (violet line) and the reference hexagonal phase submicropisms using trisodium citrate as the chelating agent (green line). As one can be seen in Fig. 3, three main emission UC peaks centered at 521, 540 and 654 nm were observed, which can be assigned to the ²H_{9/2} → ⁴I_{15/2}, the ²H_{11/2}/⁴S_{3/2} → ⁴I_{15/2} and the ²H_{9/2} → ⁴I_{15/2} transitions of Er³⁺ ions, respectively. It is noted that the position and the shape of all the emission spectra are similar, with the exclusive difference in the relative intensities between the distinct emission bands. The hexagonal phase YPO₄•0.8H₂O:18%Yb³⁺,2%Er³⁺ nanoflakes prepared at pH = 7 show the highest emission intensity, while the tetragonal phase nanoparticles prepared at pH = 3, the mixed phase nanoparticles prepared at pH = 5 and the hexagonal phase nanorod prepared at pH = 9 display the lowest intensities of similar magnitude.

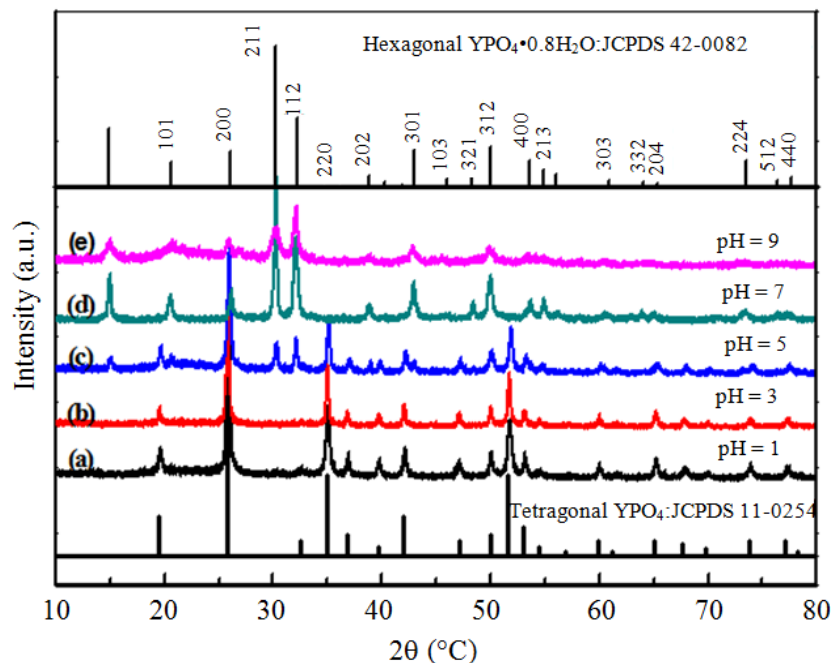


Fig. 1. The XRD patterns of the as-prepared $\text{YPO}_4:18\% \text{Yb}^{3+}, 2\% \text{Er}^{3+}$ samples at different pH values of (a) 1, (b) 3, (c) 5, (d) 7 and (e) 9. The standard XRD patterns of hexagonal phase $\text{YPO}_4 \cdot 0.8\text{H}_2\text{O}$ (JCPDS 42-0082) and tetragonal phase YPO_4 (JCPDS 11-0254) are included as references.

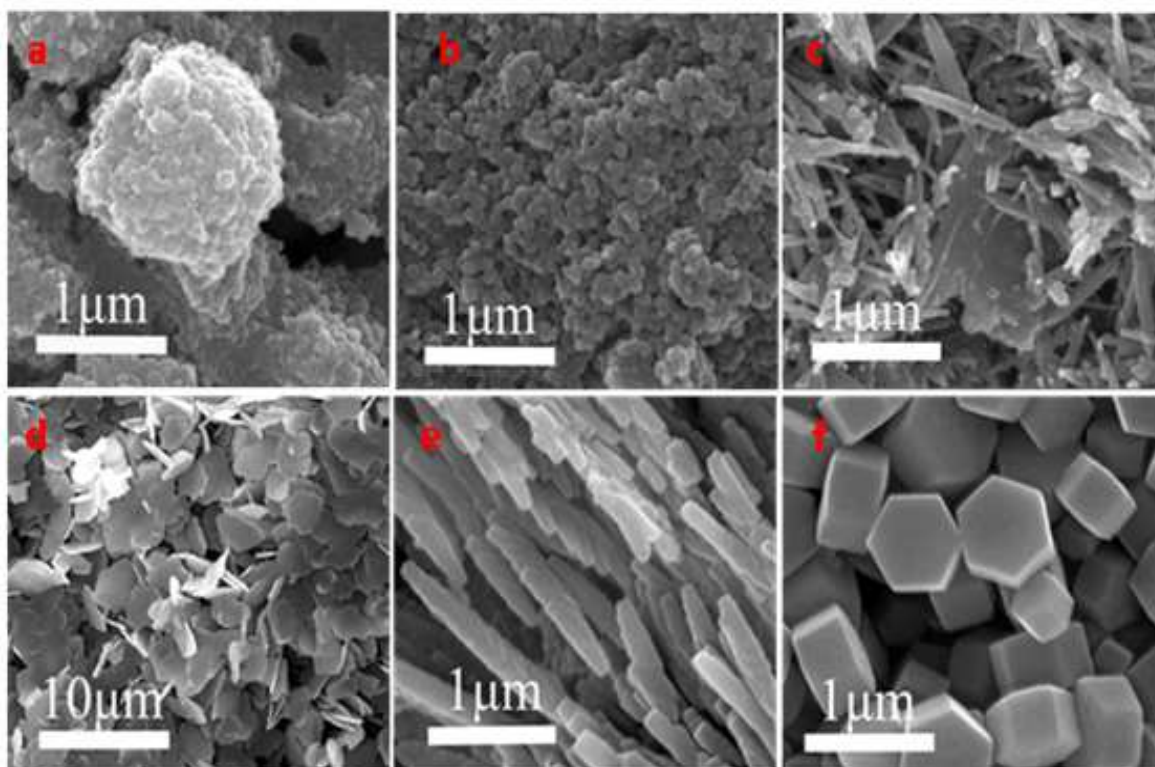


Fig. 2. FESEM images for YPO_4 and $\text{YPO}_4 \cdot 0.8\text{H}_2\text{O}:18\% \text{Yb}^{3+}, 2\% \text{Er}^{3+}$ samples prepared with different pH values using the OA as chelating agent: (a) pH = 1; (b) pH = 3; (c) pH = 5; (d) pH = 7; (e) pH = 9 and (f) trisodium citrate as chelating agent

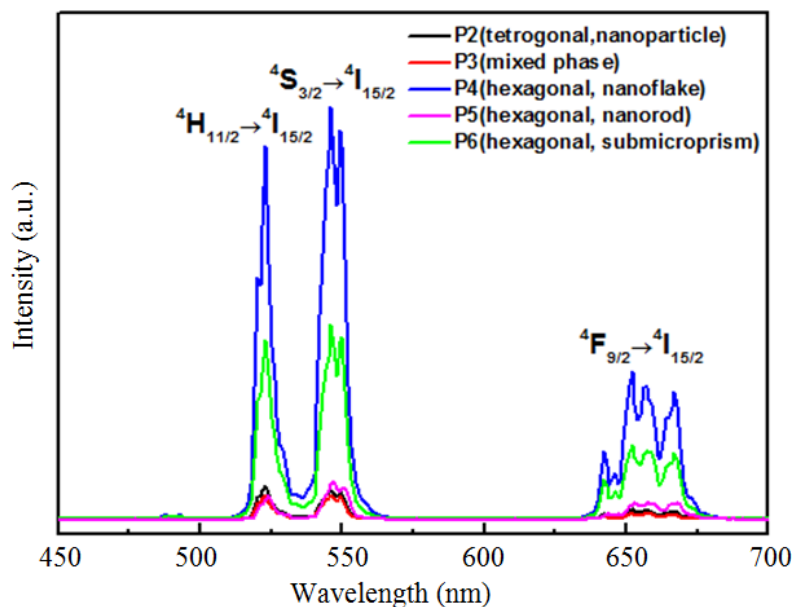


Fig. 3. UC Photoluminescence (PL) spectra of YPO_4 and $\text{YPO}_4 \cdot 0.8\text{H}_2\text{O} : 18\% \text{Yb}^{3+}, 2\% \text{Er}^{3+}$ samples with different pH values under diode laser excitation at 980 nm. Excitation power density, $\sim 390 \text{ W/cm}^2$

Furthermore, the intensity of the hexagonal phase $\text{YPO}_4 \cdot 0.8\text{H}_2\text{O} : 18\% \text{Yb}^{3+}, 2\% \text{Er}^{3+}$ nanoflakes (average 3 μm in size and 30 nm thick) prepared using the OA as chelating agent is almost 2 times as high as that of $\text{YPO}_4 \cdot 0.8\text{H}_2\text{O} : 18\% \text{Yb}^{3+}, 2\% \text{Er}^{3+}$ submicron microprisms ($\sim 700 \text{ nm}$ in size and $\sim 350 \text{ nm}$ thick) prepared using trisodium citrate as chelating agent. The difference in UC luminescence intensities among all investigated samples can be attributed to the combined roles of the phase, morphology and the particle sizes. The samples of hexagonal phase with higher crystallinity and larger size tend to emit stronger UC emission intensity. This is because (i) the smaller surface-to-volume ratio the particle processes, the fewer surface lanthanide ions will be exposed to surface quenching sites, thus the lesser the surface-related quenching effect will be created; (ii) the lower crystal phase favors the higher UC emission intensity, due to the lessened constraint on the forbidden dipole-dipole nature of the f-f transition; (iii) the higher crystalline in the resulting particles produces less crystal defects to provide quenching effects, thus favoring the UC emission intensity (Downing *et al.*, 1996; Chen *et al.*, 2013b).

In order to understand the UC mechanism of the $\text{Yb}^{3+}/\text{Er}^{3+}$ co-doped YPO_4 system, the dependence of the upconverted visible emission intensities on the laser pump power were measured and displayed in a logarithmic scale in Fig. 4. For the unsaturated conditions, the formulation $I_{\text{UC}} \propto P^n$ can be used to

quantify the number of photons that are involved for the population of the upper emitting state; where the I_{UC} is the luminescence emission intensity from the upper emitting state, P is the pump laser power and n is the number of the laser photons involved. The fitting slope of the experimental data in a double logarithmic plot can accurately provide the photon numbers, as shown in Fig. 4. For the hexagonal phase $\text{Yb}^{3+}/\text{Er}^{3+}$ co-doped YPO_4 nanoflakes prepared at $\text{pH} = 7$, the n values of 2.08, 2.03 and 1.89 were obtained for the UC emission peaks at 521 nm (green), 540 nm (green), 654 nm (red), respectively. These slope values demonstrates that a two-photon process is responsible for both the green and the red UC emissions, for $\text{Yb}^{3+}/\text{Er}^{3+}$ co-doped YPO_4 nano/microcrystals of varying morphologies and phases.

Figure 5 displays the energy levels of the Yb^{3+} and Er^{3+} as well as the proposed UC mechanisms involved to produce to the upconverted emission bands in Fig. 3. Firstly, the Yb^{3+} ion absorbs one laser photon and is excited from the ground $^2\text{F}_{7/2}$ state to the $^2\text{F}_{5/2}$ state. The release of the energy via the first $\text{Yb}^{3+} \rightarrow \text{Er}^{3+}$ energy transfer excites the Er^{3+} ions from the $^4\text{I}_{15/2}$ state to the $^4\text{I}_{11/2}$. Then, the Er^{3+} ion is further promoted to the $^4\text{F}_{7/2}$ state through a second $\text{Yb}^{3+} \rightarrow \text{Er}^{3+}$ energy transfer process. The $^2\text{H}_{11/2}$ and $^4\text{S}_{3/2}$ states can be populated by nonradiative relaxations from the $^4\text{F}_{7/2}$ state, which generate the 521 and 540 nm emissions by radiative decay to the ground state. In addition, the red emission centered at 654 nm can be

acquired through the radiative transition from the $^4F_{9/2}$ (Er^{3+}) to the $^4I_{15/2}$ (Er^{3+}) state. Here, the $^4F_{9/2}$ (Er^{3+}) state can be populated by a nonradiative decay from the $^4S_{3/2}$ state (Er^{3+}) involving the assistance of phonons from the YPO_4 host lattice. It is noted that the green upconversion emission show stronger intensity than that of the red emission. This might be attributed to the large energy gap ($\sim 3059\text{ cm}^{-1}$) between the $^4S_{3/2}$ state and the $^4F_{9/2}$ state, resulting in inefficient nonradiative deactivations to populate the $^4F_{9/2}$ state and thus producing the weak red UC emissions.

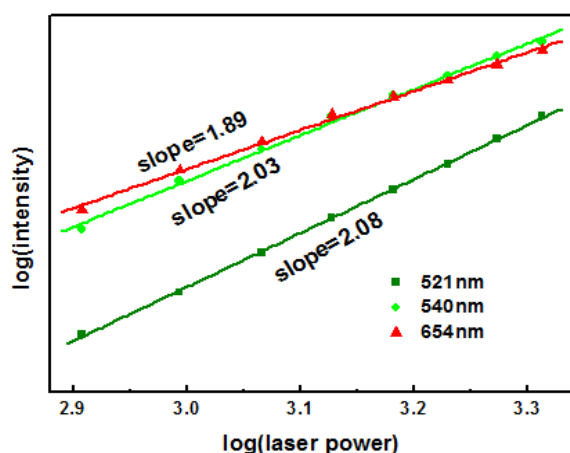


Fig. 4. A logarithmic-logarithmic plot of the dependence of the upconverted emission intensities of the bands centered at 521, 540 and 654 nm on the laser pump power, obtained from the hexagonal phase $YPO_4 \cdot 0.8H_2O: 18\%Yb^{3+}, 2\%Er^{3+}$ nanoflakes prepared at pH = 7

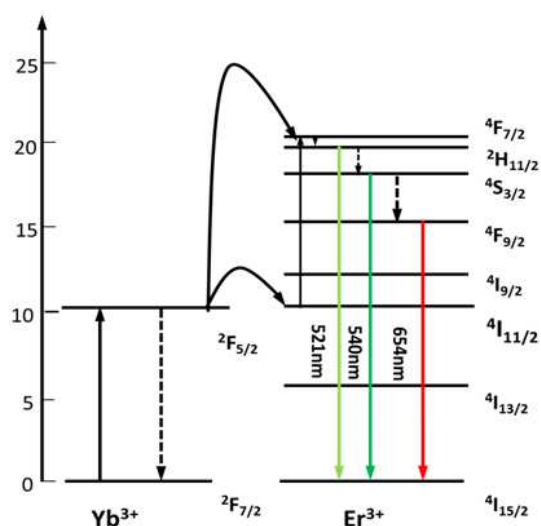


Fig. 5. The proposed energy transfer mechanisms involving the Yb^{3+} and the Er^{3+} ions, following a diode laser excitation of 980 nm

Conclusion

In summary, we have developed a facile hydrothermal route to prepare Yb^{3+}/Er^{3+} co-doped YPO_4 nano/microcrystals with pH-controlled morphologies and sizes using the OA as the chelating agent. Moreover, the YPO_4 nanoparticles, nanoflakes and nanorods can be easily obtained via simply tuning the pH value (from 1 to 9) of the reaction solution while keep all other reaction parameters the same. Moreover, a phase transformation from the tetragonal $YPO_4: 18\%Yb^{3+}, 2\%Er^{3+}$ nanoparticles to the hexagonal $YPO_4 \cdot 0.8H_2O: 18\%Yb^{3+}, 2\%Er^{3+}$ particles can also be induced by increasing the pH value from 3 to 5. Furthermore, spectroscopic investigations of the resulting particles revealed a phase-, morphology- and size-dependent UC luminescence when excited at $\sim 980\text{ nm}$. The highest UC luminescence intensity was from the hexagonal $YPO_4 \cdot 0.8H_2O: 18\%Yb^{3+}, 2\%Er^{3+}$ nanoflakes prepared at pH = 7. Additionally, the UC emission mechanism is also studied in details. This work provides a pilot investigation on developing lanthanide doped upconverting orthophosphates of varying size, phase and morphology for future photonic and biophotonic applications.

Acknowledgement

This work is supported by Natural Science Foundation of China (51402071), international scientific and technological cooperation projects (Grant No. 2014DFA50740) and the National Science Fund for Distinguished Young Scholars (Grant No. 51325201).

Author's Contributions

Meiling Tan: Performed the experiment, drafted the manuscript

Shuwei Hao: Performed the experiments, analyzed the data, edited the manuscript.

Xiangbin Meng: Performed the experiments, analyzed the data.

Jing Liu and Yunfei Shang: Data analysis.

Chunhui Yang: Developed the idea, supervised the experiments, analyzed the data, edited the manuscript

Guanying Chen: Developed the idea, supervised the experiments, analyzed the data and edited the manuscript.

Ethics

The authors would like to disclose that Dr. Guanying Chen is an editorial board member for the American Journal of Engineering and Applied Sciences.

References

- Balakrishnaiah, R., D.W. Kim, S.S. Yi, K. Jang and H.S. Lee *et al.*, 2009. Effect of Al³⁺ ions on fluorescence properties of YPO₄:Eu³⁺ phosphors. *Mater. Lett.*, 63: 2063-2066. DOI: 10.1016/j.matlet.2009.06.053
- Balakrishnaiah, R., D.W. Kim, S.S. Yi, S.H. Kim and J. Kiwan *et al.*, 2010. NIR to VIS frequency upconversion luminescence properties of Er³⁺-doped YPO₄ phosphors. *Thin Solid Films*, 518: 6145-6148.
- Chen, G., J. Shen, T.Y. Ohulchanskyy, N.J. Patel and A. Kutikov *et al.*, 2012. (alpha-NaYbF₄: Tm³⁺)/CaF₂ Core/shell nanoparticles with efficient near-infrared to near-infrared upconversion for high-contrast deep tissue bioimaging. *ACS Nano.*, 6: 8280-8287. DOI: 10.1021/nn302972r
- Chen, G., C. Yang and P. N. Prasad, 2013b. Nanophotonics and nanochemistry: Controlling the excitation dynamics for frequency up-and down-conversion in lanthanide-doped nanoparticles. *Acc. Chem. Res.*, 46: 1474-1486. DOI: 10.1021/ar300270y
- Chen, G., J. Seo, C. Yang and P.N. Prasad, 2013a. Nanochemistry and nanomaterials for photovoltaics. *Chem. Soc. Rev.*, 42: 8304-8338. DOI: 10.1039/C3CS60054H
- Chen, G., H. Qiu, P.N. Prasad and X. Chen, 2014. Upconversion nanoparticles: Design, nanochemistry and applications in theranostics. *Chem. Rev.*, 114: 5161-5214. DOI: 10.1021/cr400425h
- de Sousa Filho, P.C. and O.A. Serra, 2011. Reverse microemulsion synthesis, structure and luminescence of nanosized REPO₄:Ln³⁺ (RE = La, Y, Gd, or Yb and Ln = Eu, Tm, or Er). *J. Phys. Chem. C*, 115: 636-646. DOI: 10.1021/jp109988a
- Di, W., X. Wang, B. Chen, H. Lai and X. Zhao, 2005. Preparation, characterization and VUV luminescence property of YPO₄: Tb phosphor for a PDP. *Opt. Mater. Des.*, 27: 1386-1390. DOI: 10.1016/j.optmt.2004.10.001
- Di, W., X. Zhao, S. Lu, X. Wang and H. Zhao, 2007. Thermal and photoluminescence properties of hydrated YPO₄:Eu³⁺ nanowires. *J. Solid State Chem.*, 180: 2478-2484. DOI: 10.1016/j.jssc.2007.06.025
- Dou, Q. and Y. Zhang, 2011. Tuning of the structure and emission spectra of upconversion nanocrystals by alkali ion doping. *Langmuir*, 27: 13236-13241. DOI: 10.1021/la201910t
- Downing, E., L. Hesselink, J. Ralston and R. Macfarlane, 1996. A three-color, solid-state, three-dimensional display. *Science*, 273: 1185-1189. DOI: 10.1126/science.273.5279.1185
- Hao, S., G. Chen, H. Qiu, C. Xu and R. Fan *et al.*, 2012. Controlled growth along circumferential edge and upconverting luminescence of beta-NaYF₄: 20%Yb³⁺, 1%Er³⁺ microcrystals. *Mater. Chem. Phys.*, 137: 97-102. DOI: 10.1016/j.matchemphys.2012.08.045
- Hao, S., W. Shao, H.L. Qiu, Y.F. Shang and R.W. Fan *et al.*, 2014. Tuning the size and upconversion emission of NaYF₄:Yb³⁺/Pr³⁺ nanoparticles through Yb³⁺ doping. *RSC Adv.*, 4: 56302-56306. DOI: 10.1039/C4RA11357H
- Hou, Z.Y., C.X. Li, P.A. Ma, G.G. Li and Z.Y. Cheng *et al.*, 2011. Electrospinning preparation and drug-delivery properties of an up-conversion luminescent porous NaYF₄: Yb³⁺, Er³⁺@Silica fiber nanocomposite. *Adv. Funct. Mater.*, 21: 2356-2365. DOI: 10.1002/adfm.201100193
- Hutchison, A.J., 1999. Calcitriol, lanthanum carbonate and other new phosphate binders in the management of renal osteodystrophy. *Perit Dial. Int.*, 19: S408-S412.
- Li, C., J. Yang, Z. Quan, P. Yang and D. Kong *et al.*, 2007. Different microstructures of β-NaYF₄ fabricated by hydrothermal process: Effects of pH values and fluoride sources. *Chem. Mater.*, 19: 4933-4942. DOI: 10.1021/cm071668g
- Li, C., Z. Quan, P. Yang, S. Huang and H. Lian *et al.*, 2008. Shape-controllable synthesis and upconversion properties of lutetium fluoride (doped with Yb³⁺/Er³⁺) microcrystals by hydrothermal process. *J. Phys. Chem. C*, 112: 13395-13404. DOI: 10.1021/jp802826k
- Li, C.X., Z.Y. Hou, C.M. Zhang, P.P. Yang and G.G. Li *et al.*, 2009. Controlled synthesis of Ln³⁺ (Ln=Tb, Eu, Dy) and V⁵⁺ ion-doped YPO₄ nano-/microstructures with tunable luminescent colors. *J. Lin. Chem. Mater.*, 21: 4598-4607. DOI: 10.1021/cm901658k
- Lisiecki, R., W. Ryba-Romanowski, A. Speghini and M. Bettinelli, 2009. Luminescence spectroscopy of Er³⁺-doped and Er³⁺, Yb³⁺-codoped LaPO₄ single crystals. *J. Lumin.*, 129: 521-525. DOI: 10.1016/j.jlumin.2008.12.006
- Luwang, N.M., R.S. Ningthoujam, S.K. Srivastava and R.K. Vatsa, 2011. Disappearance and recovery of luminescence in Bi³⁺, Eu³⁺ codoped YPO₄ nanoparticles due to the presence of water molecules up to 800°C. *J. Am. Chem. Soc.*, 133: 2998-3004. DOI: 10.1021/ja1092437
- Mai, H.X., Y.M. Zhang, L.D. Sun and C.H. Yan, 2007. Orderly aligned and highly luminescent monodisperse rare-earth orthophosphate nanocrystals synthesized by a limited anion-exchange reaction. *Chem. Mater.*, 19: 4514-4522. DOI: 10.1021/cm0710731

- Meiser, F., C. Cortez and F. Caruso, 2004. Biofunctionalization of fluorescent rare-earth-doped lanthanum phosphate colloidal nanoparticles. *Angew. Chem. Int. Ed.*, 43: 5954-5957. DOI: 10.1002/anie.200460856
- Meysamy, H., K. Riwotzki, A. Kornowski, S. Naused and M. Haase, 1999. Wet-chemical synthesis of doped colloidal nanomaterials: Particles and fibers of LaPO₄:Eu, LaPO₄:Ce and LaPO₄:Ce,Tb. *Adv. Mater.*, 11: 840-844. DOI: 10.1002/(SICI)1521-4095(199907)11:10<840::AID-ADMA840>3.0.CO;2-2
- Riwotzki, K., H. Meysamy, H. Schnablegger, A. Kornowski and M. Haase, 2001. Liquid-phase synthesis of colloids and redispersible powders of strongly luminescing LaPO₄:Ce,Tb nanocrystals. *Angew. Chem. Int. Ed.*, 113: 573-576. DOI: 10.1002/1521-3773(20010202)40:3<573::AID-ANIE573>3.3.CO;2-S
- Shan, J.N., S.J. Budijono, G.H. Hu, N. Yao and Y.B. Kang *et al.*, 2011. Pegylated composite nanoparticles containing upconverting phosphors and meso-Tetraphenyl Porphine (TPP) for photodynamic therapy. *Adv. Funct. Mater.*, 2: 2488-2495. DOI: 10.1002/adfm.201002516
- Tian, G., Z.J. Gu, L.J. Zhou, W.Y. Yin and X.X. Liu *et al.*, 2012. Mn²⁺ dopant-controlled synthesis of NaYF₄:Yb/Er upconversion nanoparticles for in vivo imaging and drug delivery. *Adv. Mater.*, 24: 1226-1231. DOI: 10.1002/adma.201104741
- Yang, X.Y., X.T. Dong, T.X. Wang and G.X. Liu, 2009. Glycine-assisted hydrothermal synthesis of YPO₄:Eu³⁺ nanobundles. *Mater. Lett.*, 63: 629-631. DOI: 10.1016/j.matlet.2008.12.004
- Zhang, P., W. Steelant, M. Kumar and M. Scholfield, 2007. Versatile photosensitizers for photodynamic therapy at infrared excitation. *J. Am. Chem. Soc.*, 129: 4526-4527. DOI: 10.1021/ja0700707